MADYN 2000 Version 4.3

The following new features and improvements were introduced in version 4.3:

1. Improvements and New Features for Nonlinear Fluid Film Bearings
2. New Features for Rolling Element Bearings
3. General Spring Connection
4. Hot Spot Stability Analysis with Flexible Support
5. Evaluation according to API 617 8th Edition
6. Further Improvements

Table of content for detailed description of features:

1. Improvements and New Features for Nonlinear Fluid Film Bearings

1.1 Analysis Time

Several code improvements (improved interpolation in the field of nonlinear characteristics, improved scaling of the fields), optimised settings for the RUNGE KUTTA solver and the use of the latest MATLAB version 2016a have considerably reduced the analysis time for transient analyses with nonlinear fluid film bearings. In some case the analysis is 10 times faster than in version 4.2.

This improvement facilitates the analysis of extreme cases within reasonable time (2 to 8 hours), such as the run up of turbo-chargers with semi-floating ring bearings (= floating ring bearing with non-rotating floating ring). The outer oil film of these bearings functions as a squeeze film damper and does not have any load carrying capacity as long as the ring does not move. This leads to very thin outer oil films (the ring is very close to the bearing casing), causing many iterations for each time step, due to the high gradients of the bearing characteristics.

In the following the run up of the turbocharger in figure 1.1 with semi-floating ring bearings in figure 1.2 is shown. The assumed unbalance for the run up can be seen in fig. 1.3.
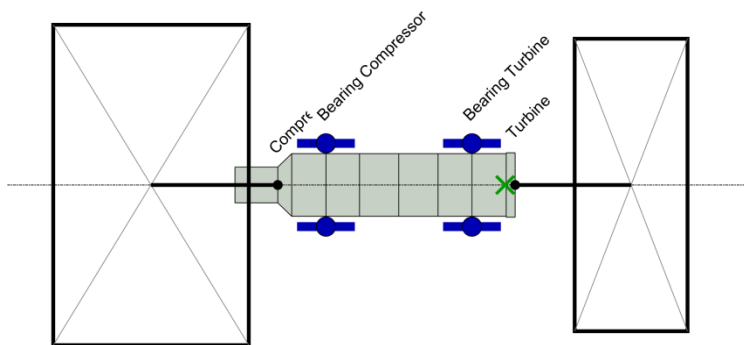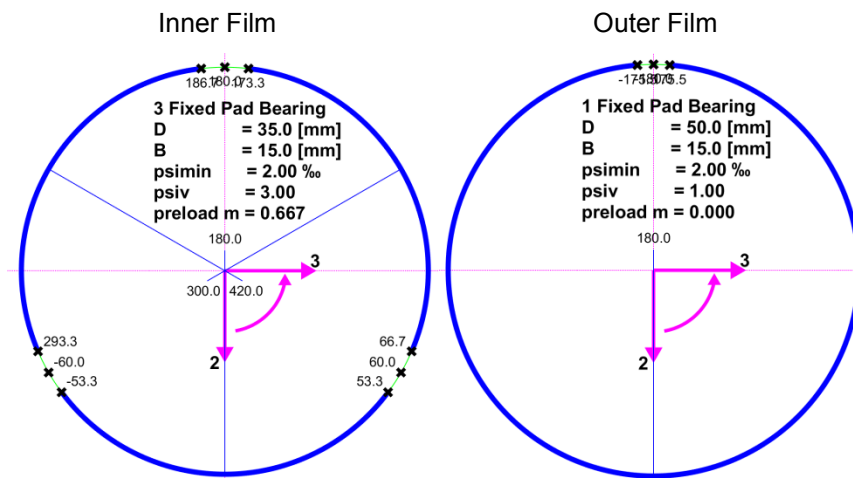

Fig. 1.1: Turbocharger example rotor

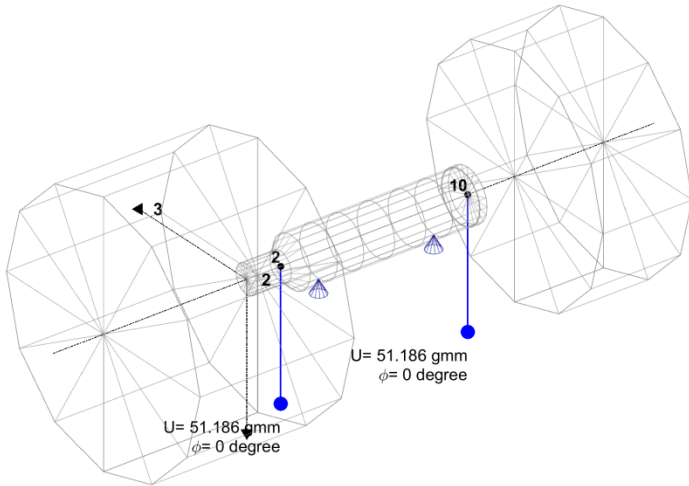Fig. 1.2: Geometry semi-floating ring bearings

Fig. 1.3: Unbalance load case for the run up according to G20

The vibration and orbit of the rings and the relative rotor vibration in the bearings are shown in figure 1.4 and 1.5. The spectrum of the vibration at the compressor wheel can be seen in figure 1.6. Figure 1.4 reveals that the ring on the heavy turbine side drops almost to a value corresponding to the clearance of the outer film. It is centred to some extent at about 27'000 rpm, the instant when sub-synchronous vibrations arise (also see spectrum in figure 1.6).
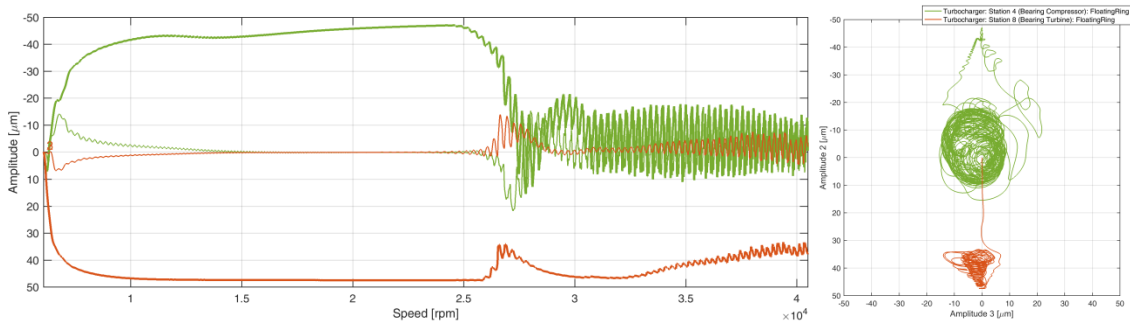

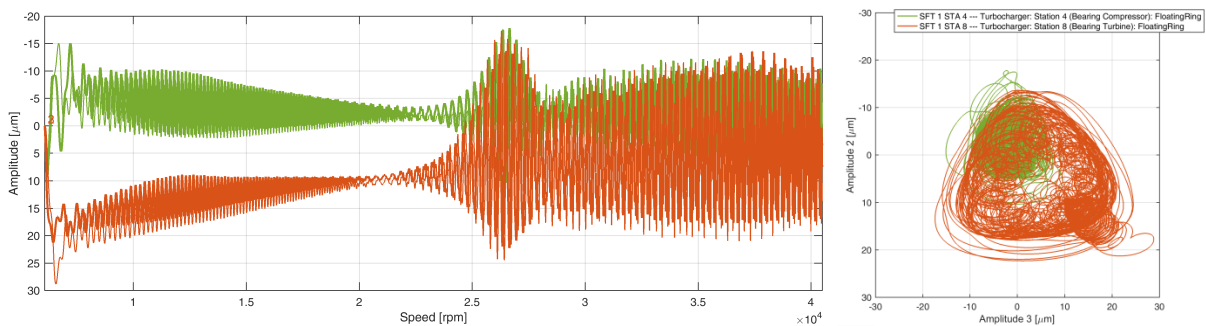Fig. 1.4: Time history and orbit of the ring

Fig. 1.5: Time history and orbit of the relative rotor vibration in the bearings
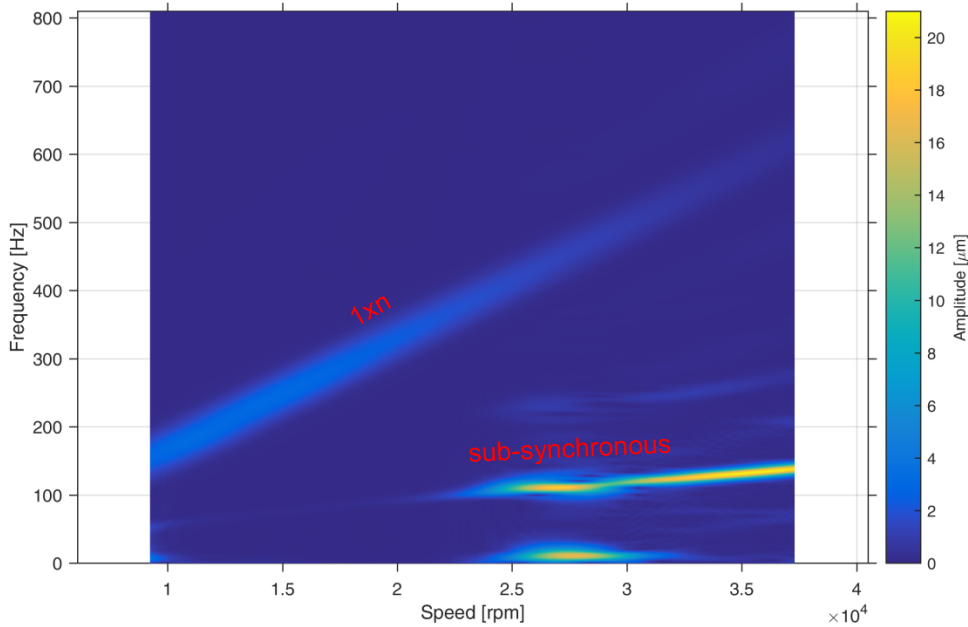
Fig. 1.6: Spectrum of the vibration at the compressor wheel

1.2 Contact Stiffness

Contact stiffness as proposed by Greenwood and Williamson[1] according to equation 1.1 is introduced for all nonlinear fluid film bearings.

$$p_c = c_a \cdot e^{C_b \cdot H} + c_c \qquad (1.1)$$

with the parameters

c_a = $556.188 \cdot 10^6 \ N/m^2$,
c_c = $-0.5285 \cdot 10^6 \ N/m^2$ and
$c_b = \frac{\ln(0.001)}{roughness}$.

The above values for c_a and c_c apply for steel. H is the oil film thickness. The surface roughness in c_b is an input in the RFB GUI (see figure 1.7).

Equation 1.1 yields a pressure distribution according to the local oil film thickness, which is added to the fluid pressure distribution.

Introducing a contact stiffness (setting the roughness to a reasonable value >0) increases the robustness of the analysis in case of deflections close to the bearing clearance.

[1] Greenwood, JA; Williamson, JBP: Contact of nominally flat surfaces. In: Proceedings of the Royal Society of London. Series A. Mathematical and Physical Sciences, 1966, vol. 295(1442), 300–319. http://rspa.royalsocietypublishing.org/content/295/1442/300.short
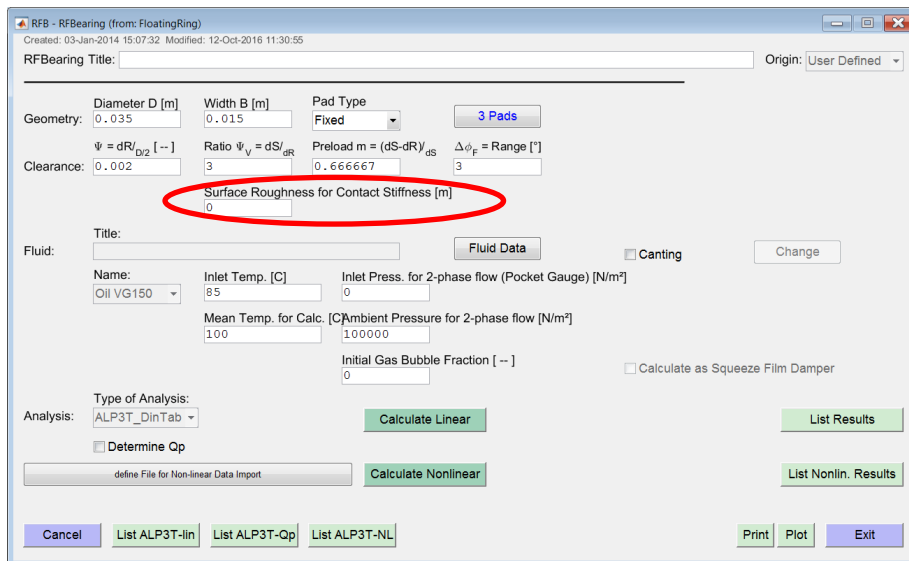
Fig. 1.7: RFB GUI with edit field for surface roughness

1.3 Thermal Deformation for Floating Ring Bearings with Stationary Ring (Semi-Floating)

Thermal deformation now can also be considered for floating ring bearings with non-rotating ring. For bearings with free rotating ring it was already possible before. The deformation influences the clearance and thus the bearing temperature. This option is available for analysis types DIN and c_ad (constant adiabatic).

In order to consider the thermal deformation the method for the "Ring Speed Ratio Calculation" must be selected accordingly in the floating ring bearing GUI (see figure 1.8).
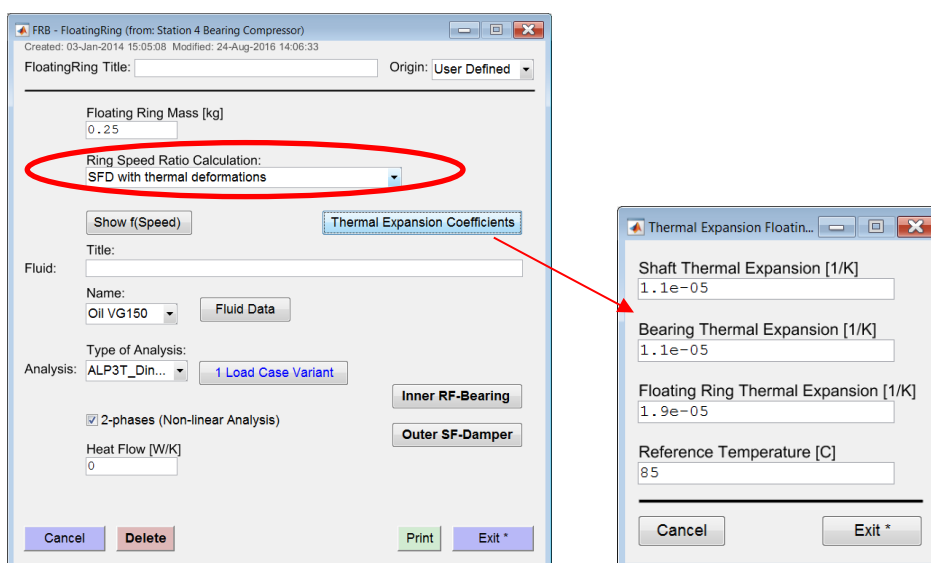
Fig. 1.8: Floating ring bearing GUI with the method for the "Ring Speed Ratio Calculation" considering the thermal ring deformation and GUI to define the thermal expansion coefficients

The speed dependent temperatures and clearance change (as ratio) can be plotted from the button "Show f(speed)". Examples for these plots are shown in figure 1.9.
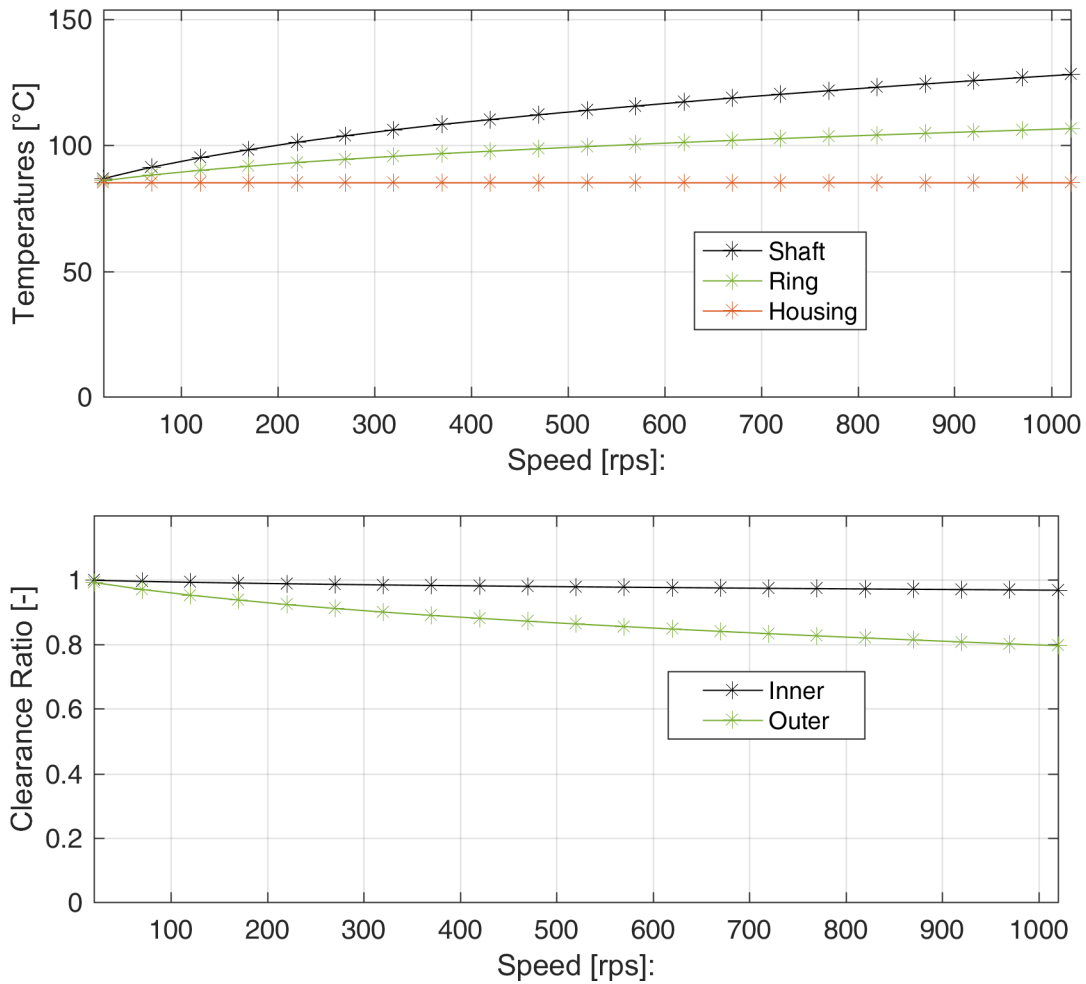

Fig. 1.9: Temperature and clearance change (as clearance ratio) as a function of speed

2. New Features for Rolling Element Bearings

2.1 Nonlinear Rolling Element Bearings

Nonlinear rolling element bearings are introduced. Clearance effects as well as the nonlinear Hertzian contact force are considered. For the analysis of the nonlinear force a function of the MESYS software is used (see https://www.mesys.ag/?page_id=1202).

The nonlinearity of the rolling element bearings has to be specified in the transient analysis GUI similar to other nonlinearities. Activating the check box "Nonlinear Solver" opens the GUI with a list of rolling element bearings REB in the system (see figure 2.1). The bearings can be enabled for the nonlinear solver.
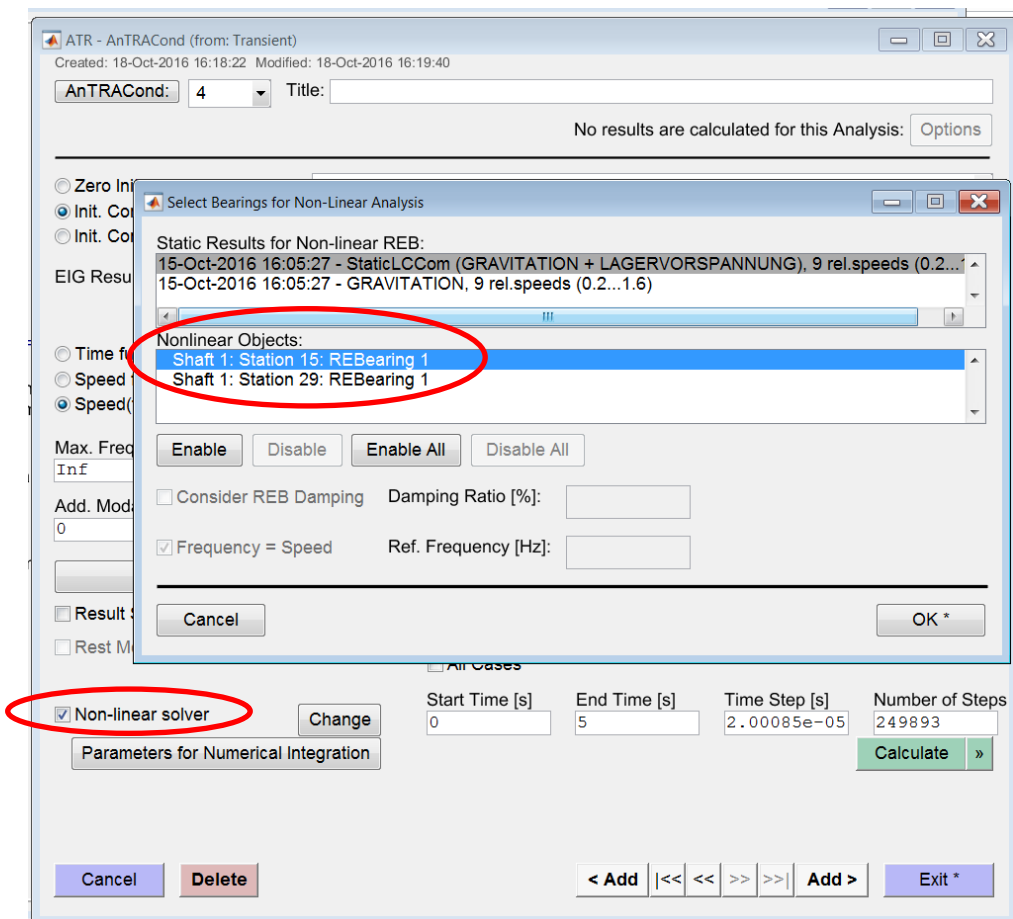
Fig. 2.1: TRA GUI with activated check box "Non-linear solver" and GUI to select REB objects

Moreover a list of static analyses is shown. They are needed to define a linear damping force, which are added to the nonlinear force from MESYS. This is described in more detail in the next chapter.

Due to nonlinear rolling element bearings especially in cases with clearance a variety of non-linear effects may arise, which will be described more in detail in a later document.

2.2 Damping in Rolling Element Bearings

Damping for nonlinear rolling element bearings

As mentioned above in chapter 2.1 damping forces (including moments) can be added to the nonlinear rolling element bearing forces. These damping forces are calculated with a matrix proportional to the linear stiffness matrix of the REB. The amount of damping is defined by a damping ratio D. The damping matrix $\boldsymbol{D}$ then is calculated according to the following formula from the REB stiffness matrix $\boldsymbol{K}$:

$$\boldsymbol{D} = \frac{2\,D}{\omega}\boldsymbol{K} \qquad\qquad (2.1)$$

ω is a reference frequency.

Damping ratio and reference frequency can be defined in the GUI for the nonlinear REB (see figure 2.1). For the reference frequency the speed can be selected alternatively to a specific frequency. The default value of a specific frequency is the nominal speed of the rotor. In order to define the linear stiffness matrix the selection of a static analysis is necessary.

Damping force for harmonic response analysis

A damping force similar to equation 2.1 can be defined for harmonic response analyses. In this case the reference frequency is equal to the excitation frequency. The damping ratio is defined in the rolling element bearing GUI (see figure 2.2).
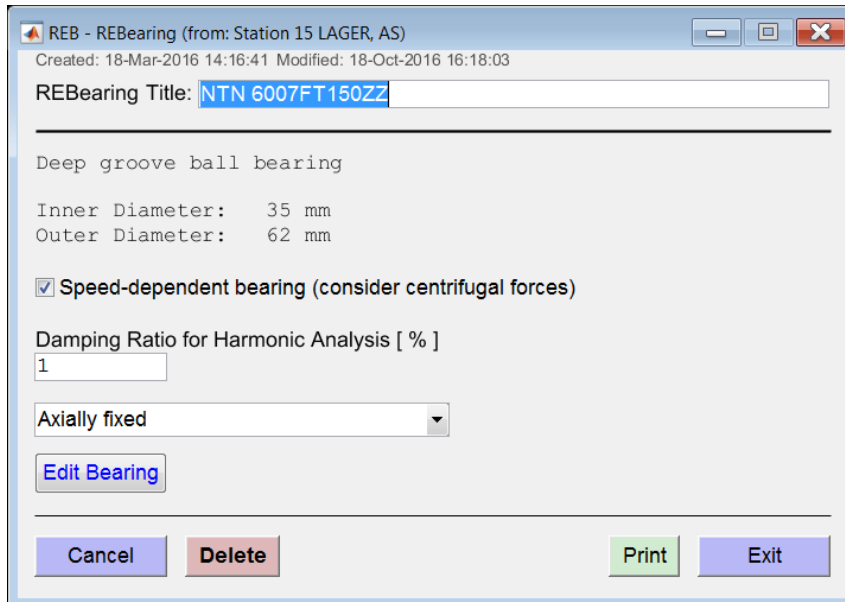

Fig. 2.2: Rolling element bearing GUI with the definition of the damping ratio for harmonic response analysis

3. General Spring Connection

General spring (6x6 stiffness and damping matrix including off-diagonals, see GUI in figure 3.1) could so far only be used as connection to the ground. It can now also be used as a connector between shafts. For this purpose a general spring has to be added to the system by the button "add General Spring" in the system GUI (see figure 3.2).
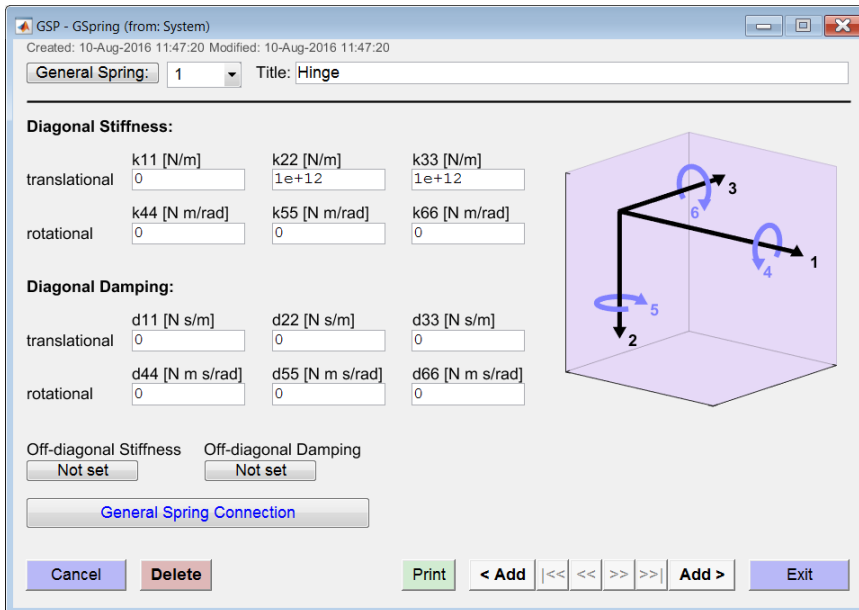

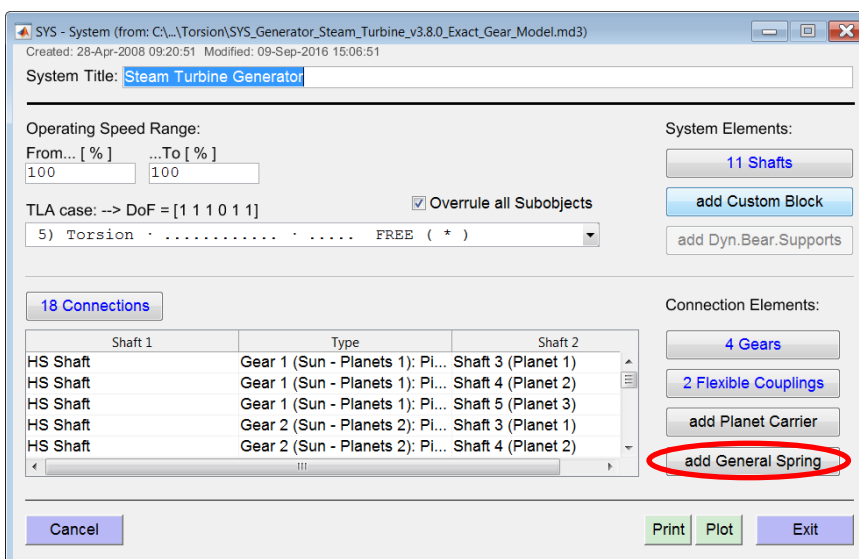Fig. 3.1: GUI to define a general spring

Fig. 3.2: System GUI with overview of connections and button to open connection GUI

General springs in the system can be used as connectors, i.e. they can be selected in the connector GUI (see figure 3.3).
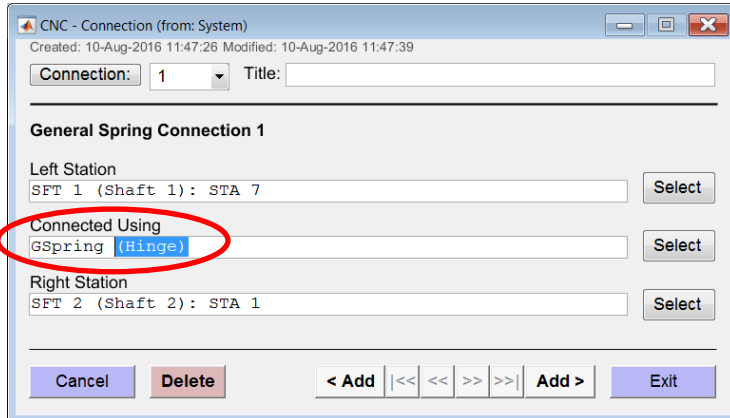
Fig. 3.3: General spring selected as connector

4. Hot Spot Stability Analysis with Flexible Support

The hot spot stability analysis now also allows flexible stators (SBS or DBS) at the hot spot location. The stator flexibility influences the heating and thus the stability. Until now only rigid stators were supported.

For the example of a turbo-expander similar to the one published in http://www.delta-js.ch/file/355/Hot_Spot_Stability_Expander.pdf the effect of a flexible stator is shown. The stiffness of the stator is about twice the fluid film bearing stiffness at nominal speed. The system is shown in figure 4.1. The Campbell diagrams with rigid and flexible stator, the mode shapes in the critical speeds with flexible stator as well as the hot spot stability charts (heat ratio curves) are shown in the following figures 4.2 to 4.6.

The flexible support has the effect of reducing the damping in the Campbell diagram. The effect on the hot spot stability threshold is large. The threshold with flexible stator is at considerable higher speed, which is due to less heating (the relative displacement in the bearing with flexible stator is smaller than with rigid stator) and the phase angles, which are more favourable regarding stability due to the smaller damping.
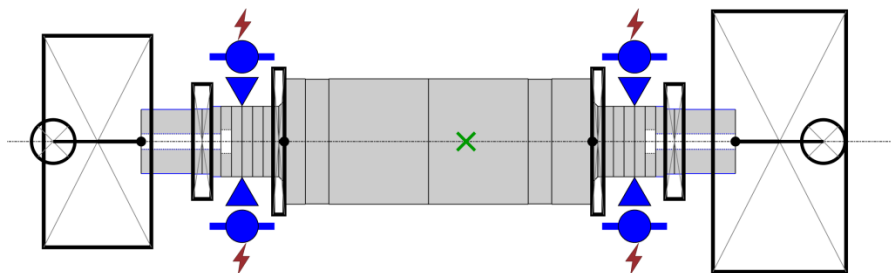
Fig. 4.1: Turbo-expander with bearing hot spots and flexible stator (SBS)

Rotor with Hot Spot (Morton Effect)

Parameter Variation Analysis
Type: Campbell Diagram
Analysis: 19-Apr-2016 09:41 - 33 rel.speeds (0.2...1.8), bearing loads from SAN

Fig. 4.2: Campbell diagram with rigid stator

Rotor with Hot Spot (Morton Effect)

Parameter Variation Analysis
Type: Campbell Diagram
Analysis: 18-Oct-2016 14:57 - 33 rel.speeds (0.2...1.8), bearing loads from SAN

Fig. 4.3: Campbell diagram with flexible stator

Rotor with Hot Spot (Morton Effect)

Parameter Variation Analysis
Type: Campbell Diagram - critical speeds only
Analysis: 18-Oct-2016 14:57 - 33 rel.speeds (0.2...1.8), bearing loads from SAN

Shape for: 3567.56 rpm
Mode: 1
Frequency: 59.48 Hz
            3568.8 cpm
Damping: 85.5 %
Whirling direction: -0.10
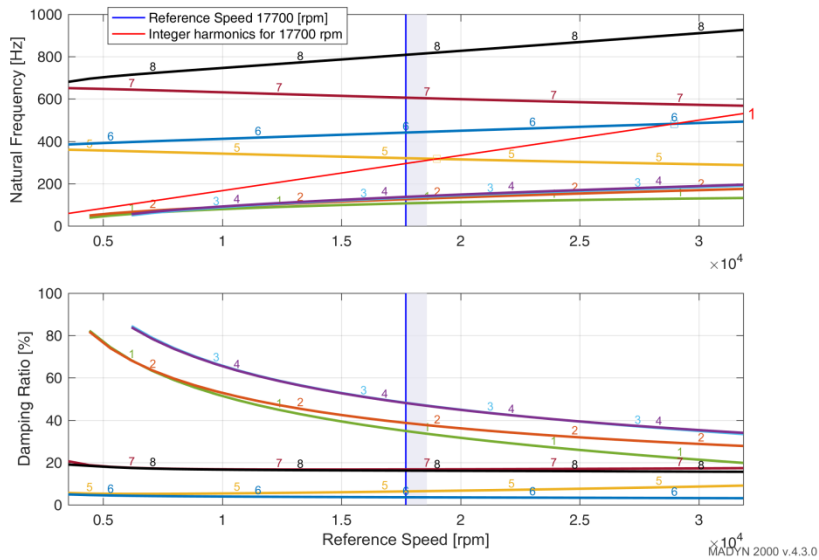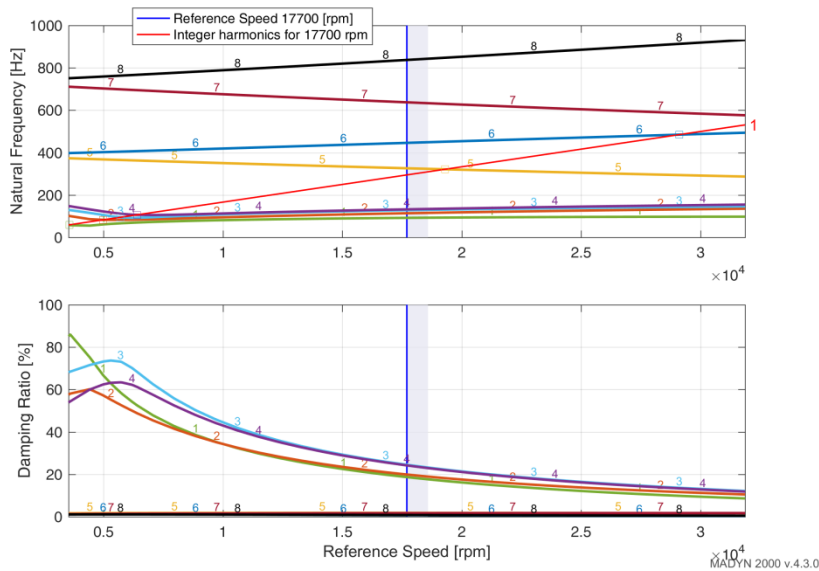Shape for: 4984.14 rpm
Mode: 2
Frequency: 83.05 Hz
            4983.0 cpm
Damping: 57.3 %
Whirling direction: +0.24
Shape for: 5705.44 rpm
Mode: 3
Frequency: 95.07 Hz
            5703.9 cpm
Damping: 73.2 %
Whirling direction: -0.08
Shape for: 6402.87 rpm
Mode: 4
Frequency: 106.69 Hz
            6401.3 cpm
Damping: 61.3 %
Whirling direction: +0.07
Shape for: 19295.72 rpm
Mode: 5
Frequency: 321.59 Hz
            19295.6 cpm
Damping: 1.8 %
Whirling direction: -1.00
Shape for: 29097.19 rpm
Mode: 6
Frequency: 484.95 Hz
            29097.2 cpm
Damping: 0.4 %
Whirling direction: +1.00
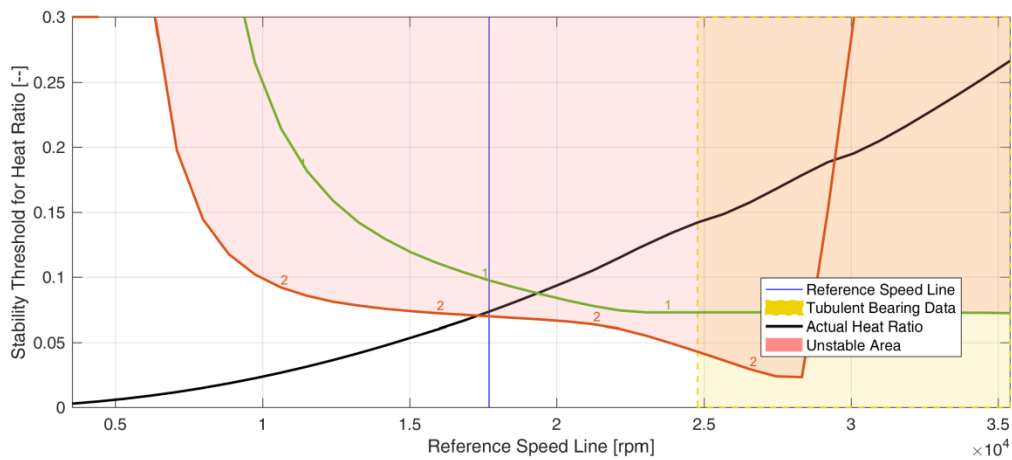
Double Overhung Rotor
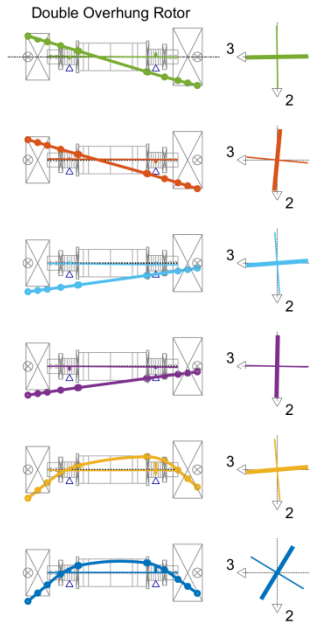
MADYN 2000 v.4.3.0

Fig. 4.4: Shapes in the critical speeds with flexible support

Rotor with Hot Spot (Morton Effect) - Stability Threshold for Heat Ratio

Hot Spot Analysis
Type: Eigenvalue Analysis
Analysis: 19-Apr-2016 09:41 - 37 rel.speeds (0.2...2), bearing loads from SAN

MADYN 2000 v.4.3.0

Fig. 4.5: Hot Spot Stability Chart with rigid support

Rotor with Hot Spot (Morton Effect) - Stability Threshold for Heat Ratio

Hot Spot Analysis
Type: Eigenvalue Analysis
Analysis: 18-Oct-2016 14:56 - 37 rel.speeds (0.2...2), bearing loads from SAN
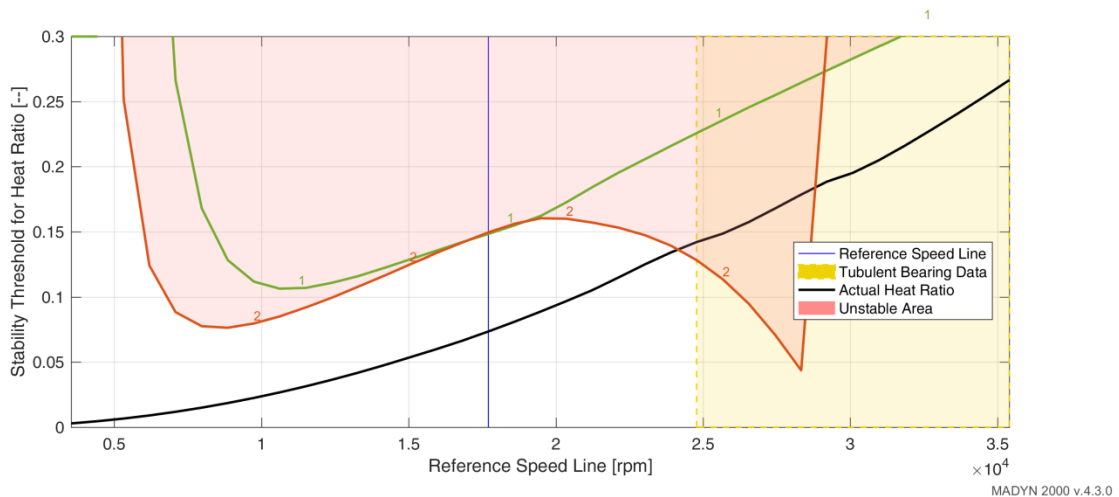

MADYN 2000 v.4.3.0

Fig. 4.5: Hot Spot Stability Chart with flexible support

5. Evaluation of Resonance Curves according to API 617 8th Edition

The evaluation of resonance curves (separation margins, amplification factors, maximum amplitudes) according to API 617 8th edition (applicable to compressors) is implemented. There are some differences to the 7th edition. The general standard API 684 (recommended practice) did not change and is still similar to API 617 7th edition.

In API 617 7th edition and API 684 the following values must be determined for resonance peaks:

Nc: Speed of the resonance peak
AF: Amplification factor
SM: Separation margin
SMreq: Required separation margin according to API
Ac: Vibration peak in the resonance
Al: Vibration limit according to API
Al/Ac: Ratio of the vibration limit to the resonance peak

Required separation margins are calculated as follows:

For critical speeds <u>below</u> minimum speed: $SM_{req} = \min\left\{17\left(1 - \frac{1}{AF-1.5}\right);\ 16\right\}$ (5.1)

For critical speeds <u>above</u> maximum speed: $SM_{req} = \min\left\{10 + 17\left(1 - \frac{1}{AF-1.5}\right);\ 26\right\}$ (5.2)

The following changes are introduced in API 617 8th edition:

For the required separation margin SM only the formulas apply. The values 16 and 26, respectively, are not used any more. This means, that for very high AF the limits are 17 and 27 instead of 16 and 26.

Instead of Ac the maximum amplitude A_{max} has to be evaluated. This evaluation has to be done in the speed range only, in contrast to Ac, which had to be evaluated for every resonance. A_{max} must not necessarily be the amplitude in a resonance; it can be the amplitude at the boundaries of the speed

range. The maximum amplitude has to be compared to the allowable amplitude, which is calculated as follows:

$$A_l = min \left\{ \frac{25.4}{2}, \frac{25.4 \sqrt{\frac{12'000}{N}}}{2} \right\} [\mu m] \tag{5.3}$$

The limitation to $\frac{25.4}{2}$ μm, which comes into effect for low speed, is new in the 8th edition.

The scaling factor S_{CC} in the 8th edition replaces the ratio A_l/Ac of the 7th edition. It is calculated as follows:

$$S_{CC} = min \left\{ \frac{A_l}{A_{max}}, 6 \right\} \tag{5.4}$$

The scaling factor must be larger than 1.

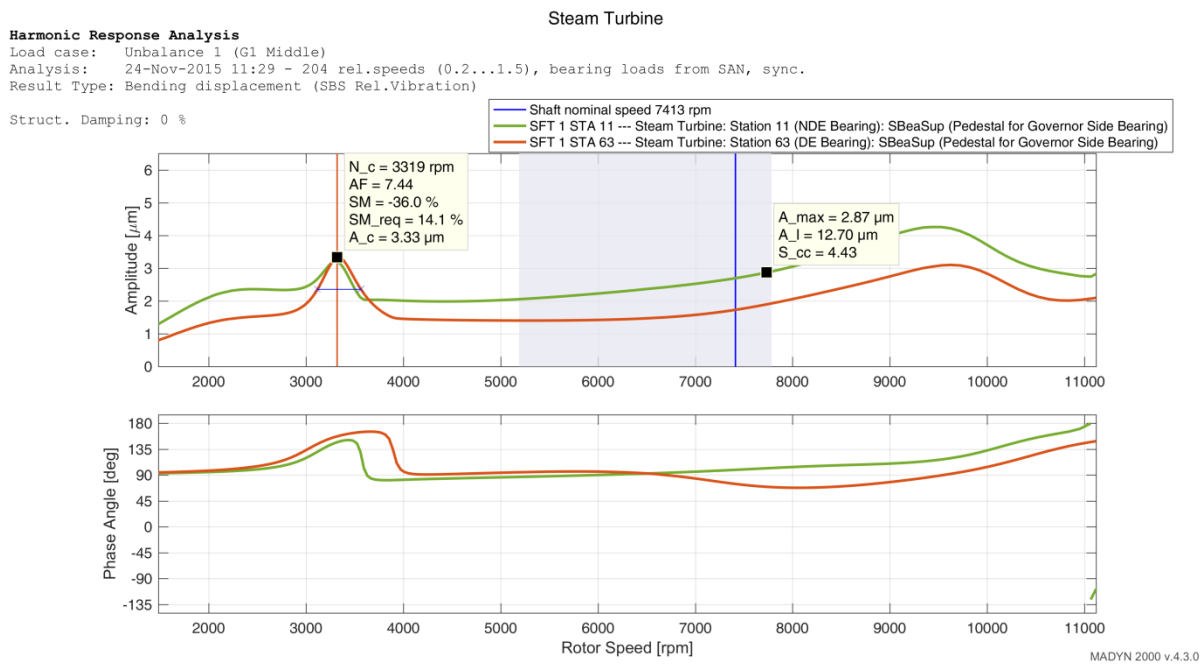The evaluation of a resonance curve according to the 8th edition is shown in the following figure.

Fig. 5.1: Evaluation of a resonance curve according to API 617, 8th edition

6. Further Improvements

6.1 Spectrograms

Spectrograms have been improved using the latest MATLAB functions and recommendations. Previously own functions were used for the correction of windowing function (Hanning). The spectrums now are much smoother as can be seen for example in figure 1.6.

6.2 Compact Mode Shape Plots for Systems with Shaft in Shaft Connections

The compact mode shape plots for systems with shaft in shaft connections have been improved. All rotors with a common axis are shown in the same shape plot. In figure 6.3 the shapes in the critical speeds for the system in figure 6.1 with two counter-rotating shafts is shown. The associated Campbell diagram can be seen in figure 6.2.
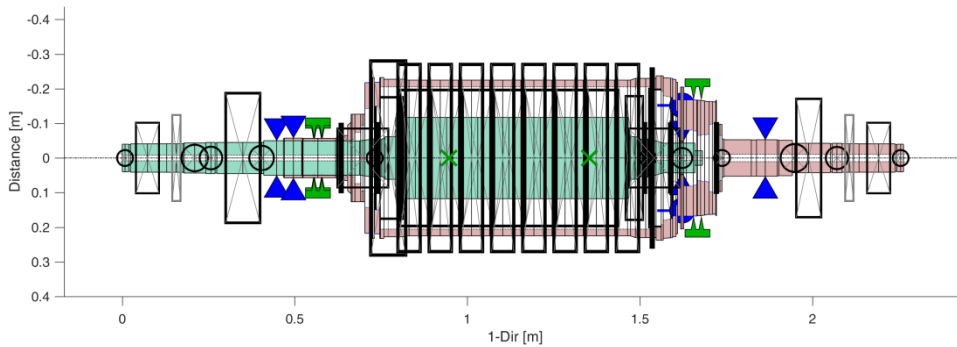

Fig. 6.1: System with shaft in shaft connection (two counter-rotating shafts)
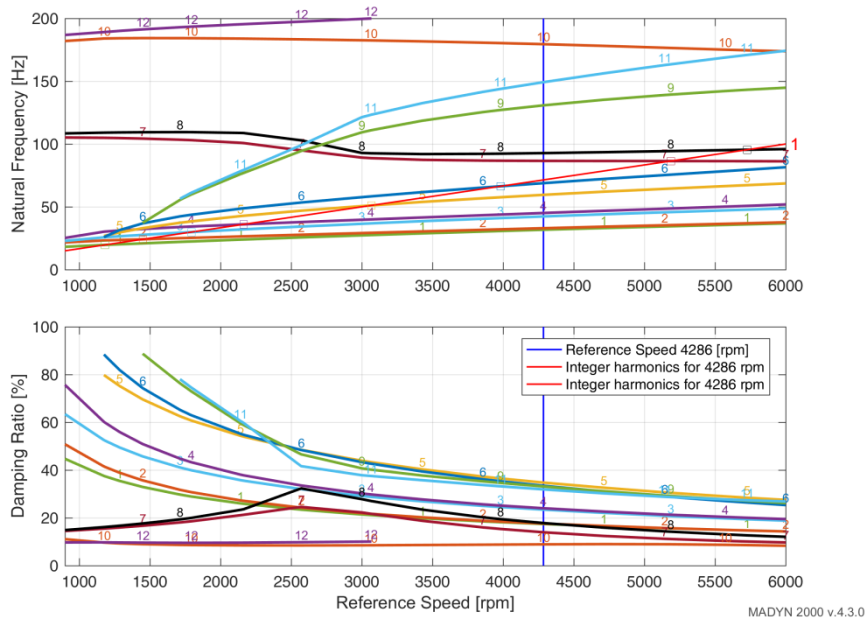
Fig. 6.2: Campbell Diagram of the system in fig. 6.1

Shape for: 935.54 rpm
Mode: 5
Frequency: 15.61 Hz
936.5 cpm
Damping: 93.3 %
Whirling direction: -0.06

Shape for: 1091.57 rpm
Mode: 6
Frequency: 18.24 Hz
1094.3 cpm
Damping: 94.4 %
Whirling direction: -0.06

Shape for: 1182.01 rpm
Mode: 1
Frequency: 19.70 Hz
1182.1 cpm
Damping: 37.4 %
Whirling direction: -0.00

Shape for: 1319.83 rpm
Mode: 9
Frequency: 22.02 Hz
1321.1 cpm
Damping: 95.9 %
Whirling direction: +0.05

Shape for: 1369.87 rpm
Mode: 11
Frequency: 22.86 Hz
1371.9 cpm
Damping: 96.1 %
Whirling direction: +0.00

Shape for: 1450.90 rpm
Mode: 2
Frequency: 24.18 Hz
1450.9 cpm
Damping: 35.7 %
Whirling direction: +0.01

Shape for: 1793.48 rpm
Mode: 3
Frequency: 29.89 Hz
1793.5 cpm
Damping: 39.9 %
Whirling direction: -0.03

Shape for: 2164.39 rpm
Mode: 4
Frequency: 36.08 Hz
2164.6 cpm
Damping: 37.8 %
Whirling direction: +0.01

Shape for: 3068.65 rpm
Mode: 5
Frequency: 51.15 Hz
3068.7 cpm
Damping: 43.3 %
Whirling direction: -0.51

Shape for: 3983.41 rpm
Mode: 6
Frequency: 66.39 Hz
3983.4 cpm
Damping: 35.3 %
Whirling direction: +0.54

Shape for: 5186.98 rpm
Mode: 7
Frequency: 86.45 Hz
5187.1 cpm
Damping: 11.1 %
Whirling direction: +0.02

Shape for: 5726.95 rpm
Mode: 8
Frequency: 95.46 Hz
5727.3 cpm
Damping: 12.7 %
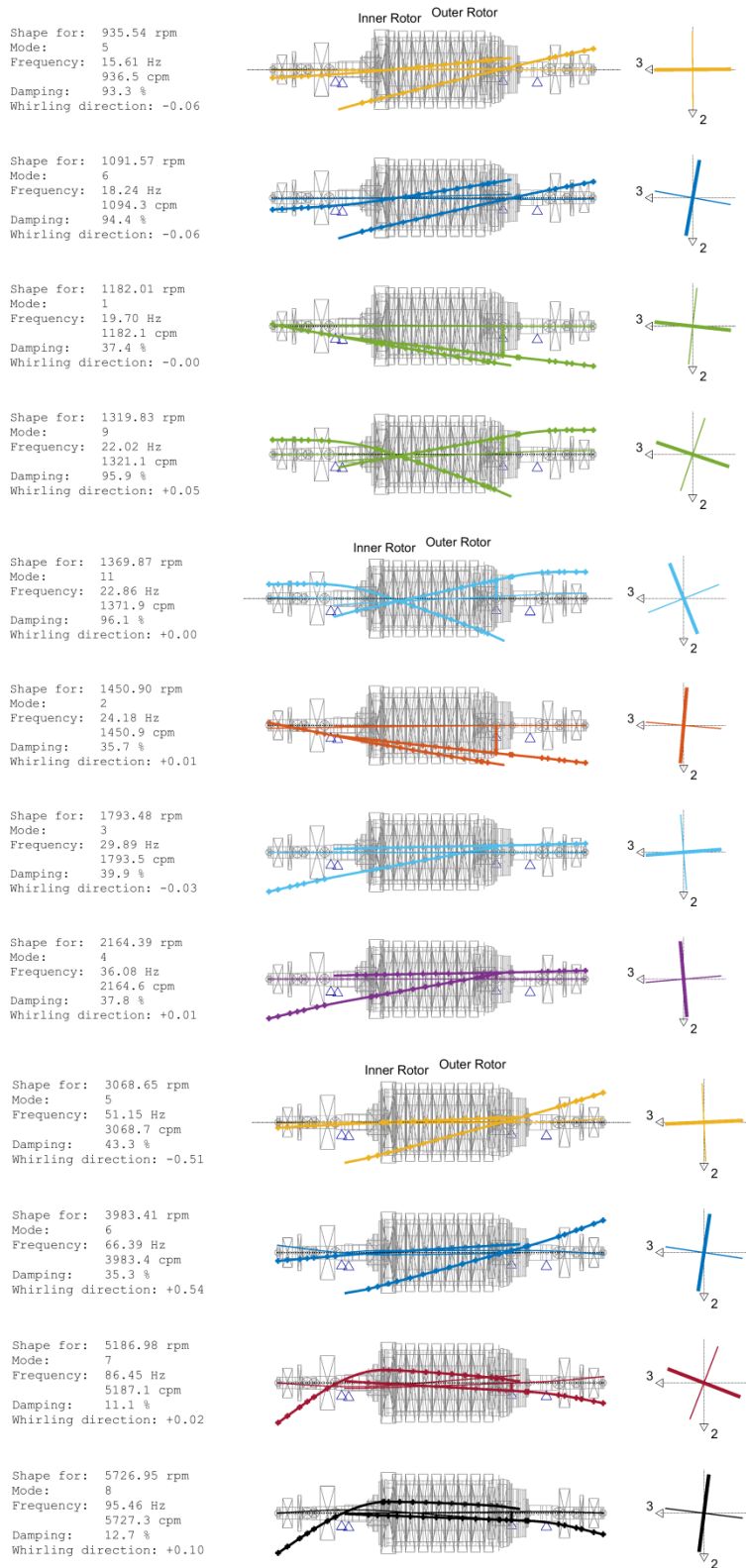Whirling direction: +0.10

Fig. 6.3: Shapes in the critical speed of the system in fig. 6.1

Compact mode shape plots of lateral, torsional, axial coupled systems have been improved as well. In case a mode is coupled the percentage of each component is shown, based on the maximum deflections of each component. For the bending the maximum among all bending coordinates (lateral displacement in direction 2,3 and rotational deflection 5,6) is considered. The bending shapes are shown in the usual way, if the shape is at least 50% bending. If the percentage of the bending is above 95% the mode is considered as dominating bending and the percentage of other component is not shown. The text with the percentage of each component can be removed by clicking on it.

For the system in figure 6.4, which is a demo-example and comes with the installation package, some coupled modes in the range of 35 to 90Hz are shown in the compact bending form (figure 6.5) and as full 3-dimensional shape plot (figure 6.6).
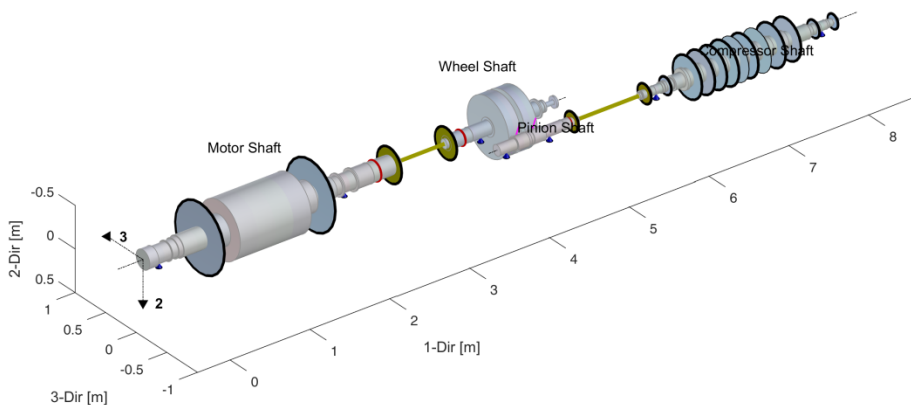

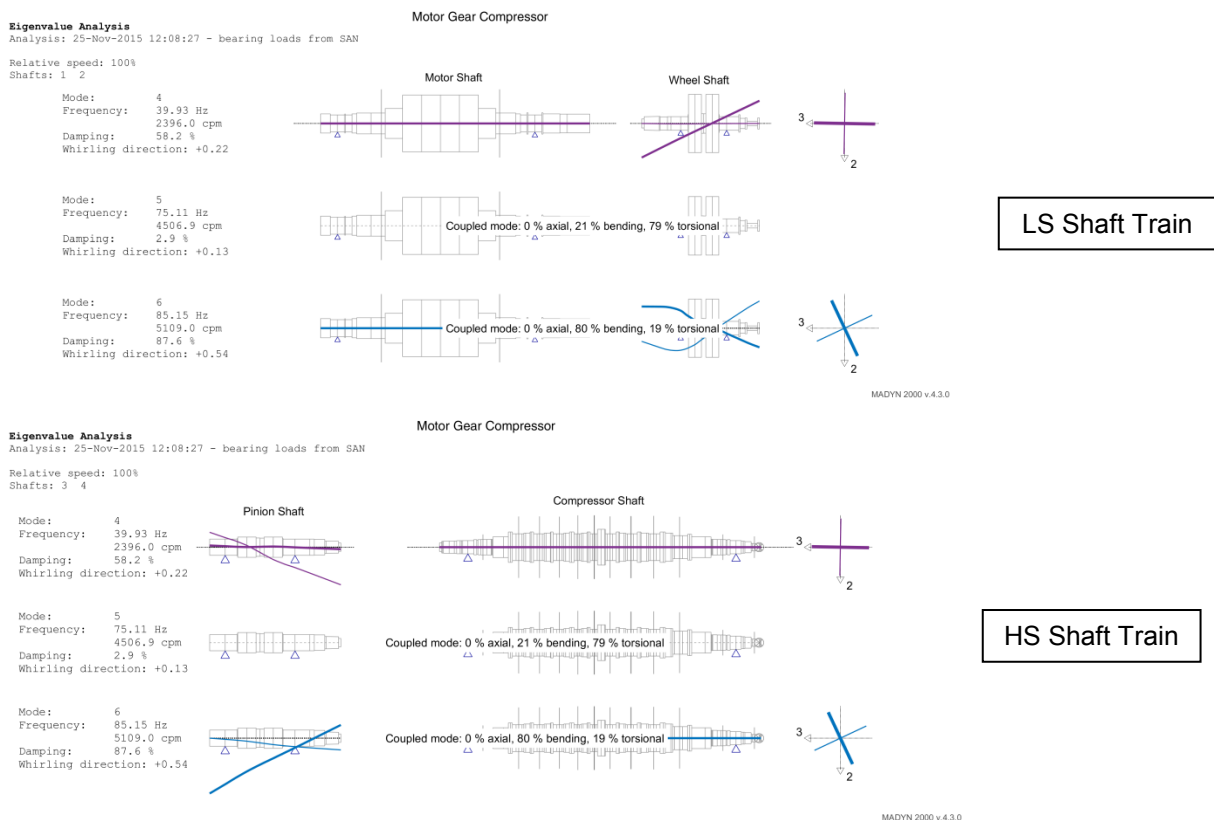Fig. 6.4: System with gear (lateral, torsional coupled)

Fig. 6.5: Compact bending mode shape plot (range 35 to 90Hz) of the coupled system in fig. 6.4
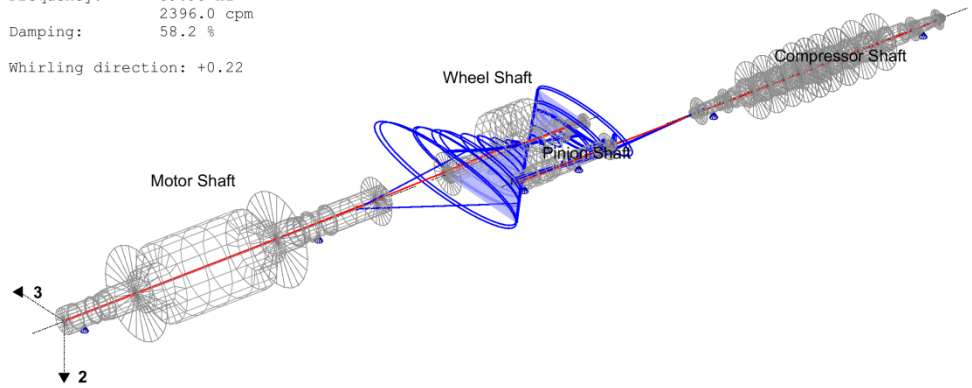
Eigenvalue Analysis
Analysis: 25-Nov-2015 12:08:27 - bearing loads from SAN

Relative speed: 100%
Mode: 4
Frequency: 39.93 Hz
               2396.0 cpm
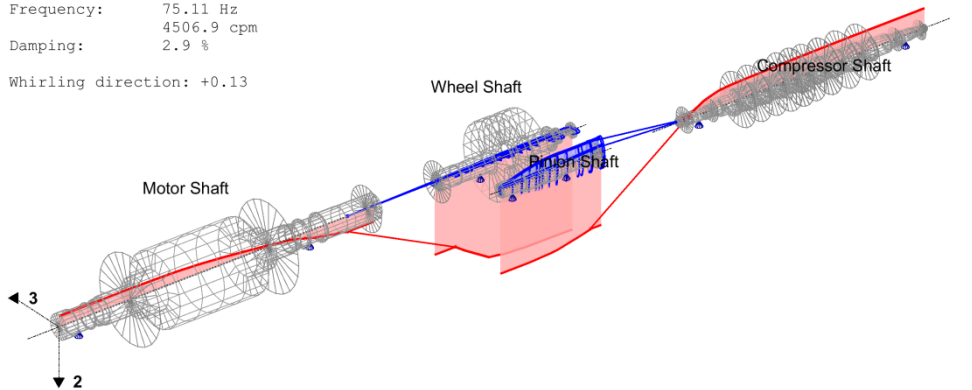Damping: 58.2 %

Whirling direction: +0.22

— Torsional angle
— Bending displacement

Compressor Shaft

Wheel Shaft

Pinion Shaft

Motor Shaft

3

2

Eigenvalue Analysis
Analysis: 25-Nov-2015 12:08:27 - bearing loads from SAN

Relative speed: 100%
Mode: 5
Frequency: 75.11 Hz
               4506.9 cpm
Damping: 2.9 %

Whirling direction: +0.13

— Torsional angle
— Bending displacement

Compressor Shaft

Wheel Shaft

Pinion Shaft

Motor Shaft

3

2

Eigenvalue Analysis
Analysis: 25-Nov-2015 12:08:27 - bearing loads from SAN

Relative speed: 100%
Mode: 6
Frequency: 85.15 Hz
               5109.0 cpm
Damping: 87.6 %

Whirling direction: +0.54

— Torsional angle
— Bending displacement

Compressor Shaft
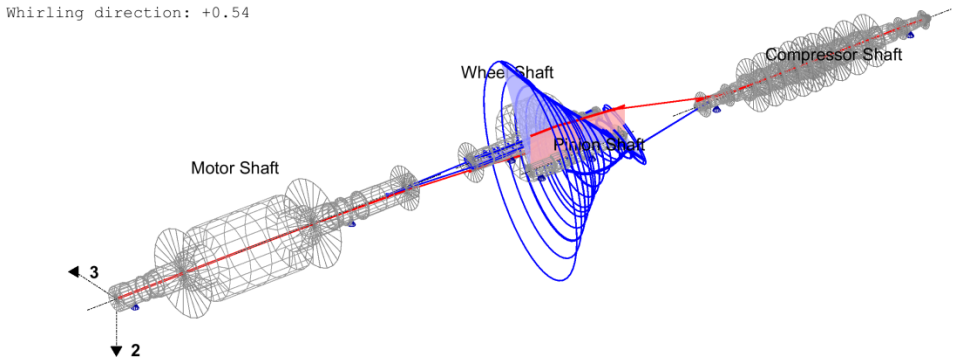
Wheel Shaft

Pinion Shaft

Motor Shaft

3

2

Fig. 6.5: Full 3-D mode shape plots (range 35 to 90Hz) of the coupled system in fig. 6.4